Chapter 3

Structures of cationic surfactant-DNA complexes

3.1 Introduction

This chapter deals with the structures exhibited by complexes of DNA with cetyltrimethylammonium bromide (CTAB) and with mixtures of CTAB and sodium-3-hydroxy-2-naphthoate (SHN). Detailed x-ray diffraction experiments have been carried out on complexes of DNA with mixtures of double-tailed cationic lipids like dioleoyltrimethylammonium propane (DOTAP) and neutral lipids like dioleoylphosphatidyl choline (DOPC) or dioleoylphosphatidyl ethanolamine (DOPE) in recent years, motivated by their potential biomedical applications. These are summarized in section 3.2. Complexation of DNA with the single-tailed cationic surfactant CTAB has been widely made use of in the extraction of DNA from plants. Nevertheless, no detailed studies have been reported on this system. CTAB forms cylindrical micelles in aqueous solution, unlike the double-tailed DOTAP, which forms bilayers. Hence CTAB-DNA complexes can be expected to form structures different from those exhibited by DOTAP-DOPC-DNA complexes. We have carried out x-ray and optical microscopy studies of CTAB-DNA complexes. These experiments described in section 3.3, reveal that the complexes have a two-dimensional (2D) hexagonal structure. However, there are two molecular packings that can result in such a lattice. In order to distinguish between these two possibilities, we have modelled the electron densities in these two structures and calculated the intensities of the diffraction peaks. This analysis, pre-

sented in section 3.4, clearly shows that the structure consists of DNA strands intercalated between cylindrical CTAB micelles. In section 3.5, we describe the structural modifications of CTAB-DNA complexes induced by the addition of SHN. We find that the structure of the complex changes from hexagonal to lamellar at a critical SHN concentration, very close to that at which a cylinder to bilayer transformation is found in the CTAB-SHN-water system. This observation further confirms the structure of the hexagonal complexes obtained from a modelling procedure. These experimental results are discussed in section 3.6. Finally, the conclusions drawn from the experiments described in this chapter are given in section 3.7 .

3.2 Earlier studies on surfactant-DNA complexes

Many of the earlier studies have been on DNA-cationic lipid systems. The earliest structure proposed in these systems, consists of liposomes attached to the DNA strands and known as the bead-on-string structure [1, 2]. Electron Microscopy studies have reported a variety of structures including oligolamellar structures [3] and tube like images indicating lipid bilayer covered DNA [4].

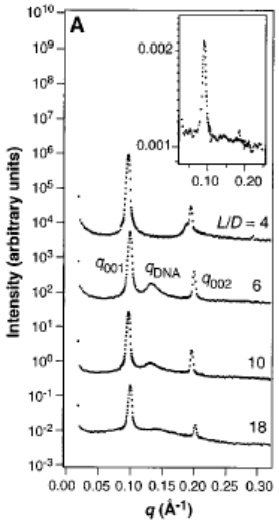

Figure 3.1: A series of SAXS scans of cationic lipid-DNA complexes in excess water as a function of different lipid to DNA weight ratio (L/D) [5]

Detailed x-ray diffraction studies [5, 6] have been carried out on complexes of DNA with

mixtures of cationic lipids like DOTAP or dimyristoyltrimethylammonium propane (DMTAP) and neutral lipids like DOPC or DOPE. In the absence of DNA, x-ray studies on the dilute, equimolar lipid mixtures did not reveal any peaks in the small angle region indicating that the bilayer separations are larger than 10 nm. However in the presence of DNA, birefringent condensates coexist with a dilute aqueous solution. These complexes were studied for different values of ρ (= weight of cationic lipid/ weight of DNA). X-ray diffraction studies on these condensates (fig 3.1) reveal a set of peaks that correspond to a lamellar periodicity of 6.51 nm and an additional diffuse peak. As the DNA concentration is increased, ie for $\rho < \rho_{iso}$ (the concentration at the isoelectric point, where the negative charges on the DNA are neutralized by the positive charges of the cationic lipid), the position of the diffuse peak shifts from 4.4 nm to 3.7 nm. Based on these observations, a structure has been proposed, where the DNA is sandwiched between the cationic lipid bilayers (fig. 3.2) known as the intercalated lamellar phase (L_α^C) [5]. The bilayer thickness is around 3.9 nm and the diameter of DNA with a hydration shell is around 2.5 nm. Hence the DNA sandwiched between two bilayers would correspond to a periodicity of about 6.4 nm, which is consistent with the periodicities observed in these complexes. The diffused peak indicates positional correlations of the DNA strands in the plane of the bilayers. The shift in the DNA-DNA peak with DNA concentration arises due to an abrupt change in the separation between the DNA strands (d_{DNA}) across the isoelectric point. There are no transbilayer positional correlations of the DNA strands when the bilayers are in the fluid L_α phase. The DNA chains confined between the bilayers form a 2D smectic [7]. At lower temperatures, when the bilayers are in the $L_{\beta'}$ phase and hence more rigid, positional correlations arise across the bilayers and a 2D rectangular lattice (fig 3.3) of the DNA has been reported [8].

d_{DNA} can be calculated from the lamellar structure proposed for the complexes, if it is assumed that all the DNA strands are adsorbed between the bilayers at ρ_{iso} [5]. If ρ_D and ρ_L are the densities of DNA and lipid respectively, δ_m the membrane thickness, A_D the area of cross-section of a DNA double helix, L and D the weights of lipid and DNA respectively,

then the separation between the DNA strands,

$$d_{DNA} = (A_D \rho_D / \delta_m \rho_L)(L/D) \tag{3.1}$$

If the amounts of cationic lipid and DNA are fixed at ρ_{iso} and (L/D) is varied by changing the amount of the neutral lipid, then according to eqn 3.1, plot of d_{DNA} vs (L/D) must be linear. This was found to agree remarkably well with the variation of d_{DNA} observed on diluting the charge of the lipid membrane by the addition of a neutral lipid [5].

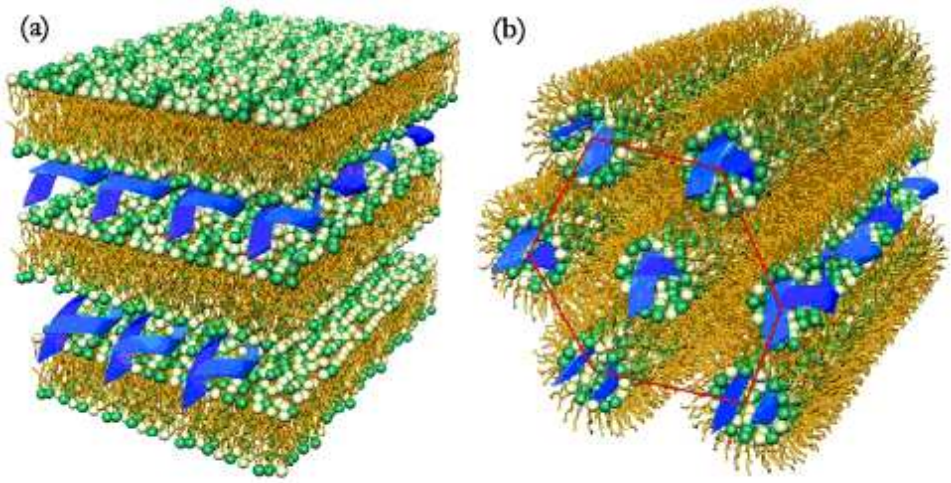

Figure 3.2: Proposed structures of the intercalated lamellar phase (a) and the inverted hexagonal phase (b) in lipid-DNA complexes [12].

Theoretical studies indicate that a variety of structures is possible in lamellar DNA-lipid complexes, like the isotropic lamellar, nematic lamellar, columnar, and sliding columnar phases, depending on the degree of ordering of the DNA strands [9]. In the isotropic lamellar phase, there is no long range or quasi long range positional or orientational order of the DNA strands. If long range orientational order arises between the DNA strands with no positional order, a nematic lamellar phase is obtained. In addition to the orientational order, when there are long range positional correlations between the DNA strands across the bilayers, we have a columnar phase with the DNA arranged on a 2D rectangular or a 2D centered rectangular lattice. The former structure results when the effective interactions between the DNA strands sandwiched between the bilayers is attractive. A centered rectangular phase

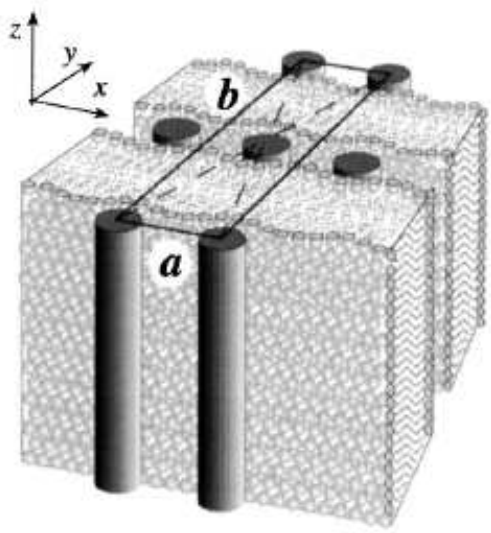

Figure 3.3: Local structure of the centered rectangular columnar DNA lattice embedded in a cationic lipid lamellar phase observed when the bilayers are in the L'_β phase [8].

would be observed when there is a repulsion between the DNA strands. Such a phase has been observed in some lipid-DNA systems as discussed above [8]. In addition to these, a sliding columnar phase has also been proposed with properties intermediate between the columnar and nematic lamellar phases. Here, in-plane smectic correlations decay as exp(-ln^2r) as a function of the DNA-DNA separation r. The positional correlation between these smectic lattices, die off exponentially with layer-number difference. Though it is very likely that the intercalated lamellar phase (L_α^C) is a sliding columnar phase, further confirmation would require monodomain samples. However to our knowledge such a phase has not yet been experimentally observed.

In lipid-DNA complexes, one would a priori expect that the separation between the DNA strands (d_{DNA}) would be determined by the isoelectric point, where the charges of the cationic lipid are neutralized by the charges on the DNA. Hence d_{DNA} should remain fixed at d_{DNA}^{iso} determined by the sample geometry [10].

$$d_{DNA}^{iso} = (A_D\rho_D/\delta_m\rho_L)(\rho_{iso}/(1-\phi_{PC})) \tag{3.2}$$

where ϕ_{PC} (=weight of DOPC/total weight of the lipid).

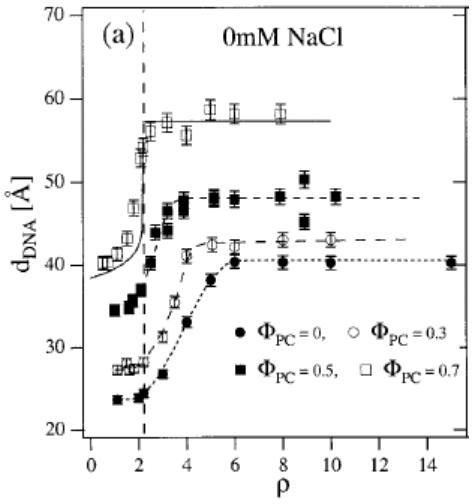

Figure 3.4: Variation of DNA packing with ρ in complexes with fixed ϕ_{PC} and no salt [10].Vertical dashed line indicates isoelectric point. The solid line through the data at ϕ_{PC} = 0.7 is the result of nonlinear Poisson-Boltzmann theory for complexes with low membrane charge density [11]

To verify this, d_{DNA} was measured for DOTAP-DOPC-DNA complexes at different values of ϕ_{PC} and ρ [10]. Microscopic observations confirm that the complex remains monophasic with no excess DNA or liposomes. The plot of d_{DNA} vs ρ at different values of ϕ_{PC} (fig 3.4) indicates an overall increase of d_{DNA} on increasing ϕ_{PC} due to the decrease in the bilayer charge density. The plot of d_{DNA} vs ρ follows the predicted behaviour only for $\rho = \rho_{iso}$ (= 2.2) (fig. 3.5). It is found that for $\rho \neq \rho_{iso}$ d_{DNA} deviates from d_{DNA}^{iso}. The complex structure has smaller d_{DNA} for $\rho < 2.2$ and a larger value of d_{DNA} for $\rho > 2.2$ (fig.3.4). However the structure remains constant away from the isoelectric point with fixed d and d_{DNA}. Electrophoresis experiments also show that complex is negatively charged for $\rho < 2.2$ and positively charged for $\rho > 2.2$.

The charge reversal of the complex at the isoelectric point implies that it absorbs excess cationic lipid when $\rho > \rho_{iso}$ and excess DNA when $\rho < \rho_{iso}$. A unit cell of the complex consists of a DNA strand of unit length and a bilayer of area d_{DNA}. The free energy per unit cell of a complex that acquires a positive charge by incorporating excess cationic lipid is

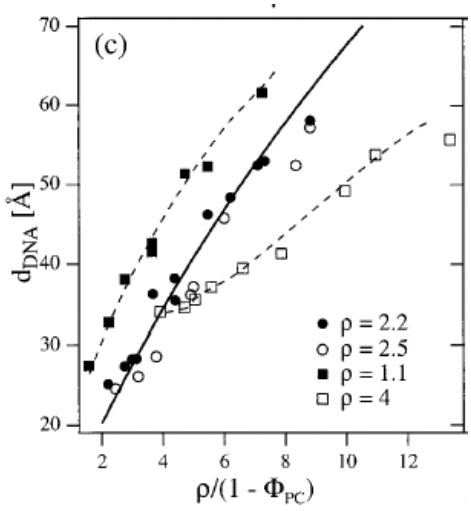

Figure 3.5: Variation of d_{DNA} with changing ϕ_{PC} in complexes with different fixed ρ. Solid line is the prediction from the geometry for isoelectric complexes [10].

given by [10]

$$F_C^+ = d_{DNA}[(1/e)(4k_BT\sigma^+)(ln(2l_D/l_C) - 1) + \pi k_BT/l_B\delta_w] \tag{3.3}$$

where $\sigma^+ = \sigma_c(1 - d_{DNA}^{iso}/d_{DNA})$ is the excess cationic charge density of the complex, σ_c the charge density of the free bilayer, e the elementary charge, k_B the Boltzmann constant and T the temperature. The first term corresponds to the free energy of the bilayer surface in the complex consisting of excess cationic lipids. The Chapman length l_C (= e/2 π σ^+ l_B), corresponds to the thickness of condensed counterion layer near the membrane surface and the Debye screening length $l_D >> l_C$. The Bjerrum length $l_B = e^2/\epsilon k_B$T . The second term corresponds to the repulsion between the bilayers. δ_w is the thickness of the water layer in the complex.

The free energy of excess cationic membrane of length d_{DNA} in the aqueous solution is given by,

$$F_B = d_{DNA}[(1/e)(4k_BT\sigma_c)(ln(2l_D/l_C) - 1)] \tag{3.4}$$

Since $\sigma^+ < \sigma_c$, the free energy of bilayer is higher in the aqueous solution than in the complex. The complex thus absorbs excess bilayer into it and lowers the free energy of the system by releasing the counterions into the complex. However the intake of cationic lipid is limited by the repulsion between the bilayers given by the second term in eqn (3.3). Also,

higher the charge density σ_c, of the bilayer, greater the amount of charged lipid which enters the complex. This was found to agree with the experimental observations.

For $\rho < \rho_{iso}$, the electrostatic energy per unit cell of the negatively charged complex is given by

$$F_C^- = \delta_w[(1/e)(4k_BT\sigma^-)(ln(2l_D/l_C) - 1) + \pi k_BT/l_B d_{DNA}] \tag{3.5}$$

where $\sigma^- = \sigma_{DNA}(1 - d_{DNA}/d_{DNA}^{iso})$ is the excess anionic charge density in the complex and σ_{DNA}, the charge density of free DNA.

The free energy per unit length of free DNA is higher in solution than in the complex. The entropy of the counterions is lower for the free DNA since they are confined near the cylindrical surface. Since σ^- is lower than σ_{DNA}, the overall free energy of the system may be lowered by incorporating the free DNA into the complex. The intake of DNA is however limited by the repulsion between the DNA strands given by the second term in equation 3.5. In fig 3.5 the data points above ρ_{iso} line corresponds to complexes which have taken in excess DNA and those below ρ_{iso} line correspond to complexes with excess lipid. Thus the shift in the d_{DNA} curves from the predicted values at ρ_{iso}, confirms the overcharging phenomenon discussed above.

The structural changes of lipid-DNA complexes, on replacing the neutral lipid DOPC by DOPE, has been studied using x-ray diffraction [12]. At low values of ϕ_{DOPE} (= weight of DOPE/total weight of the lipid), diffraction peaks indicate a lamellar structure for the complex similar to that observed in DOTAP-DOPC-DNA complexes. At $\phi_{DOPE} = 0.75$, four peaks are obtained (fig 3.6) which can be indexed as the (1 0), (1 1), (2 0) and (2 1) peaks of a 2D hexagonal lattice. The lattice parameter was found to be 6.74 nm. The DOPE-DOTAP bilayer thickness is around 4 nm. Also, pure DOPE forms an inverted hexagonal phase (H_{II}) in excess water [13, 14]. The observed lattice parameter of 6.8 nm is consistent with an inverted hexagonal structure (H_{II}^C) shown in fig 3.2 with a lipid monolayer thickness of 2 nm,

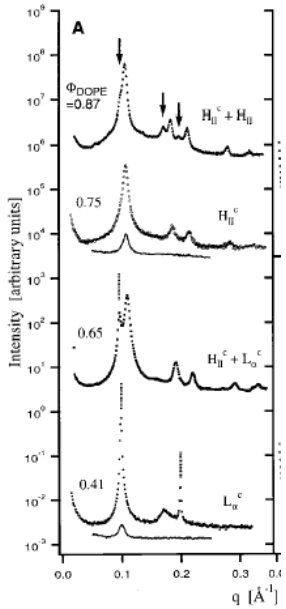

Figure 3.6: SAXS scans of cationic lipid-DNA complexes as a function of increasing ϕ_{DOPE} [12].

and an aqueous core of 2.8 nm diameter. Such a core can accommodate a DNA strand with two hydration shells.

The structure of the complex is determined by the elastic properties of the lipid membrane and the electrostatic interactions between the lipid and the DNA [15, 16]. In the inverted hexagonal phase, the neutralization of the negative charges on the DNA by the cationic lipids is more efficient as compared to L_α^C, since the lipids are brought closer to the DNA strands in the former structure. But the bending of the lipid monolayer around the DNA in H_{II}^C phase, costs energy. The presence of DOPE in the complex however leads to a negative spontaneous curvature of the lipid-water interface and reduces this energy cost. Hence the addition of DOPE to DOTAP-DNA complexes induces a structural transformation from L_α^C to H_{II}^C.

Systematic studies similar to those discussed above on cationic lipid- DNA systems have not been carried out on complexes of single-chained cationic surfactants with DNA. This is despite the fact that the complexation with such a cationic surfactant CTAB, is often

used for RNA and DNA extraction from plants [17]. It is also being used for quick extraction of high quality DNA from lambda phages [18]. Various techniques have been used to study cationic surfactant-DNA complexes. But not many structural investigations have been carried out. Complex formation between short DNA fragments (200 bp) and dodecyltrimethylammonium bromide (DTAB) has been studied using dynamic light scattering (DLS), static light scattering (SLS), high performance capillary electrophoresis (HPCE) and DTAB-specific electrode [19]. Light scattering studies indicate that the diffusion coefficient of the complexes decrease in a non-linear manner as the degree of binding of surfactant ions (determined using a surfactant selective electrode) increases, and attains saturation at 0.8 molecules of surfactants per DNA phosphate group. Using HPCE, electrophoretic mobility of DNA has been measured as a function of free surfactant concentration. Comparison of the diffusion coefficient of complexes with their electrophoretic mobility suggests that the decrease in mobility is caused by an increase in the hydrodynamic friction, as more surfactant molecules are bound without changing the effective charge of DNA. Further increase in surfactant concentration leads to a significant decrease in mobility. This is due to the effective neutralization of the DNA. Hence the complex formation occurs in two stages. In the first stage, surfactant cations exchange with the counterions condensed on the surface of the DNA, without changing the effective charge on the DNA. More surfactant molecules bind in the second stage, causing a charge neutralization of the DNA and phase separation of the complex [19]. The effects of binding at surfactant concentrations below the critical micellar concentration has also been examined [20] using techniques like spectroscopy, fluorescence, isothermal titration calorimetry, high-resolution ultrasonic velocity and density measurements. It was found that the binding of surfactants results in a significant change in the DNA secondary structure. Fluorescence studies have also reported a discrete transition from an elongated coil to a collapsed globule of a single DNA (166 kbp) molecule in the presence of a cationic surfactant [21].

There have been some x-ray studies to probe the structure of single-tailed cationic

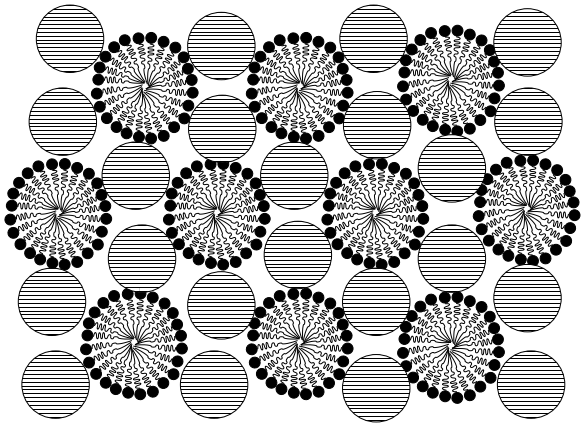

Figure 3.7: Schematic of the structure of the intercalated hexagonal phase, where each DNA strand is surrounded by three cylindrical micelles. The lattice parameter, $a = \sqrt{3}\,(R_m + R_{DNA})$, where R_m is the radius of the cylindrical micelle (~ 2.0 nm) and R_{DNA} that of the hydrated DNA strand (~ 1.25 nm)

surfactant–DNA complexes [22]. The surfactants used were DTAB, tetradecyltrimethylammonium bromide (TTAB), CTAB and octadecyltrimethylammonium bromide (OTAB). OTAB did not form complexes with DNA. The x-ray diffraction studies of DNA complexed with DTAB, show one peak at 3.6 nm. The TTAB-DNA complexes show peaks at 4 nm and 2.25 nm, which may be indexed as the (1 0) and (1 1) reflections of a 2D hexagonal lattice. Two peaks were also obtained for CTAB-DNA complexes at 4.4 nm and 2.54 nm which may again be indexed on a 2D hexagonal lattice. However in these studies, the peaks at 2.25 nm for the TTAB-DNA and 2.54 nm for CTAB-DNA complexes were wrongly attributed to the DNA-DNA separation within the complexes. Based on these observations, a structure was proposed for the complex, where the DNA strands are intercalated between the micellar aggregates, forming a 2D hexagonal lattice (fig.3.7). The model was proposed on the basis that the surfactants as well as DNA form a hexagonal phase at higher concentrations and not from any detailed analysis of the diffraction data. An inverted hexagonal phase as seen in DNA-lipid complexes cannot be be ruled out from these studies. Hence we found it necessary to carry out further studies on these complexes to determine their structure unambiguously.

3.3 Structure of CTAB-DNA complex

CTAB solutions of appropriate concentrations were prepared in deionized water (Millipore). On adding DNA to the surfactant solution, the complex precipitates out. It was left to equilibriate in solution for about 4 days. The complex was then examined under a polarizing microscope and found to be birefringent. On heating, it was found to be stable up to 90°*C*. The precipitate along with some supernatant was transferred into a 1 mm diameter glass capillary for x-ray studies. The x-ray diffraction of the CTAB-DNA complex gives 3 peaks in the small angle region of the diffraction pattern (fig 3.8) with the magnitude of the scattering vectors q in the ratio $1 : \sqrt{3} : 2$. We index them as the (1 0), (1 1) and (2 0) reflections from a 2D hexagonal lattice. The relative integrated intensities of the 3 reflections after geometric corrections, are in the ratio $1 : 0.07 \pm 0.02 : 0.013 \pm 0.003$. Relative intensities and the peak positions were found to be independent of the DNA concentration and of CTAB concentration up to 300 mM . Though x-ray diffraction determines the lattice of the complex, two possible structures can be proposed. One of them is an inverted hexagonal phase, where the DNA strands coated by a surfactant monolayer are arranged on a 2D hexagonal lattice (fig 3.2). A similar structure has been observed in lipid-DNA complexes [12]. The other is the intercalated phase (fig 3.7) consisting of DNA strands intercalated into the direct hexagonal phase of CTAB, where each DNA strand is surrounded by three cylindrical micelles [22].

The lattice parameter for the CTAB-DNA complex is 5.64±0.09 nm. Taking the thickness of CTAB bilayer δ_s to be 3 nm and the radius of the hydrated DNA strand, R_{DNA} to be 1.25 nm, inverted phase would give a lattice parameter a ($=\delta_s + 2.R_{DNA}$) ~ 5.5 nm. If the radius of the cylindrical micelle R_m is 1.98 nm, the intercalated phase would have a lattice parameter a, given by $\sqrt{3}(R_m + R_{DNA})$ ~ 5.6 nm. Hence neither of the structures can be ruled out on the basis of the lattice parameter obtained for the complex. Intercalated phase would ensure that the complex is hydrophilic, whereas inverted phase would make it hydrophobic. Complexes of CTAB with short DNA are found to form stable dispersions which might lead

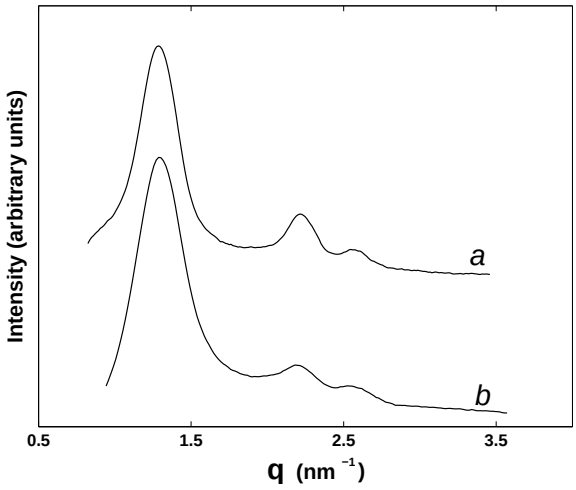

Figure 3.8: Diffraction patterns of the CTAB-DNA complex. ρ (=weight of CTAB/weight of polyelectrolyte) for the different curves are: 1.0 (a); 7.2 (b); CTAB concentration in the aqueous solution was 10 mM.

us to suspect that it forms an intercalated phase [23]. But this may not be conclusive of the structure. Only three reflections are obtained in the diffraction pattern of these systems with our experimental conditions, and hence the structure cannot be determined by calculating electron density maps. We have, therefore, used a modelling approach to determine the structure.

3.4 Modelling the structure of CTAB-DNA complex

To distinguish between the two distinct structures possible in CTAB-DNA complexes, as discussed above, we constructed models for the electron densities of each of these structures. The relative intensities calculated from the two models were then compared with the experimentally observed values.

The two dimensional electron density $\rho(\mathbf{r})$ of these two structures can be written as a convolution of a lattice function $\rho_L(\mathbf{r})$, which represents a 2D array of delta functions corresponding to the hexagonal lattice, with the electron density $\rho_b(\mathbf{r})$ as the repeating basis. [24].

Table 3.1: The parameters for the models obtained from the literature [25].

parameters	values
r_c	1.58 nm
ρ_c	0.28
ρ_w	0.332
r_h	0.4 nm
ρ_h	0.352

$$\rho(\mathbf{r}) = \rho_L(\mathbf{r}) \otimes \rho_b(\mathbf{r}) \tag{3.6}$$

where **r** is a 2D vector.

The observed diffraction intensity I(**q**), where **q** is the scattering vector, is given by

$$I(\mathbf{q}) = A|F(\mathbf{q})|^2 = A|F_L(\mathbf{q})|^2|F_b(\mathbf{q})|^2 \tag{3.7}$$

where $F(\mathbf{q})$, $F_L(\mathbf{q})$ and $F_b(\mathbf{q})$ are the fourier transforms of $\rho(\mathbf{r})$, $\rho_L(\mathbf{r})$ and $\rho_b(\mathbf{r})$, respectively, and A is a constant independent of **q**. In these models (fig 3.9), the DNA strand is represented as a circular disc of uniform electron density ρ_D. ρ_D has contributions from the water molecules and from the counterions present in the complex. The radius r_D of the disc is taken to be that of a DNA molecule with a hydration shell around it (= 1.25 nm). Each cylindrical micelle is represented as a cylindrical disc of uniform electron density ρ_c and radius r_c corresponding to the chain region, surrounded by an annular ring of electron density ρ_h and width r_h representing the head group of the micelle. The inverted micelle is modelled as an annular ring of electron density ρ_h and width r_h, surrounding the circular disc representing the DNA molecule. The values of electron density of water ρ_w, ρ_c, ρ_h, r_h and r_c taken from the literature [25] are given in table 3.1.

$\rho_b(\mathbf{r})$ for the intercalated phase is given as

$$\rho_b(r,\theta) = \rho_{DNA}(r) \otimes [\delta(\theta)\delta(r-b) + \delta(\theta-\pi)\delta(r-b)] + \rho_m(r) \tag{3.8}$$

where b is the separation between the DNA and the micellar cylinder and θ is the angle

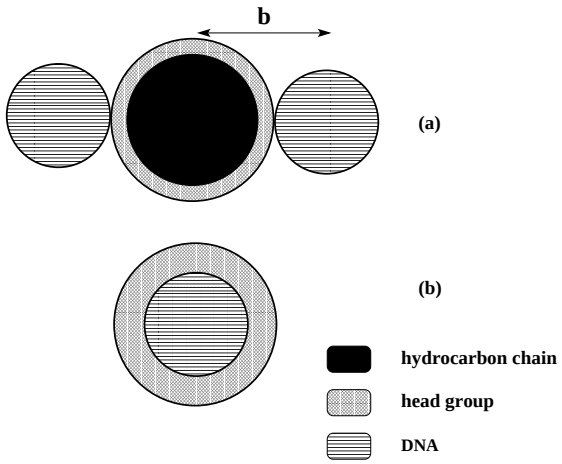

Figure 3.9: The repeating basis in the intercalated (a) and inverted (b) hexagonal phases.

made by b with the x-axis (fig 3.9). $\rho_m(r)$ and $\rho_{DNA}(r)$ are the electron densities of the cylindrical micelle and DNA strand respectively.

$$\rho_{DNA}(r) = \rho_D - \rho_w, 0 < r < r_D$$
$$=0, r > r_D$$
$$\rho_m(r) = \rho_c - \rho_w, 0 < r < r_c$$
$$= \rho_h - \rho_w, r_c < r < r_c + r_h$$
$$= 0, r > r_c + r_h$$

Fourier transforming $\rho_b(r, \theta)$, we get

$$F(q, \phi) = 4\pi cos[qb(cos\phi)]\rho_D r_D J_1(qr_D)/q + F_m(q) \tag{3.9}$$

where ϕ is the angle made by **q** with the x-axis and $J_1(qr_D)$ is the Bessel function of order 1. $F_m(q)$, the form factor of the micelle is given by

$$F_m(q) = 2\pi\rho_h[(r_h + r_c)J_1(q(r_h + r_c))/q - r_c J_1(qr_c)/q] \tag{3.10}$$

$\rho_b(\mathbf{r})$ of the inverted phase is,

$$\rho_b(r) = \rho_D - \rho_c, 0 < r < r_D$$

$$= \rho_h - \rho_c, r_D < r < r_h + r_D \tag{3.11}$$

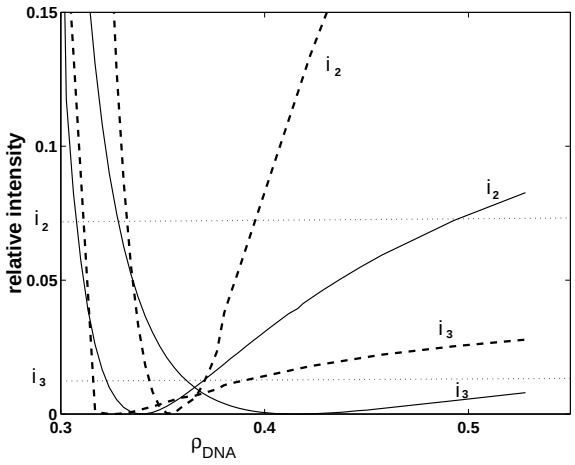

Figure 3.10: Variation of the relative intensities of the second and third Bragg peaks with ρ_{DNA}, obtained from the model for the intercalated (dashed lines) and inverted hexagonal phases (solid lines) of CTAB-DNA complex. The dotted lines indicate the experimental values of the relative intensities.

Fourier transforming $\rho_b(r)$, we get

$$F(q) = 2\pi\rho_D r_D J_1(qr_D)/q + 2\pi\rho_h[(r_D + r_h)J_1(q(r_D + r_h))/q - r_D J_1(qr_D)/q] \qquad (3.12)$$

The relative intensities of the (1 0), (1 1) and (2 0) reflections of the hexagonal phase can be calculated using equation 3.7.

Due to the different contributions to ρ_D mentioned earlier, it could not be estimated. Therefore the relative intensities of the (1 1) and (2 0) reflections with respect to that of the (1 0) reflection denoted as i_2 and i_3 respectively were calculated from the two models for a reasonable range of values of ρ_D (fig 3.10). As seen from the figure, only in the case of the intercalated hexagonal phase the calculated and observed intensities match for a particular value of ρ_D, thus confirming the structure. Hence we conclude from these studies that CTAB-DNA complexes form an intercalated phase. The formation of an intercalated phase suggests that the structure in the complex is determined by the morphology of the aggregates in the surfactant solution. To ascertain this we have tuned the spontaneous curvature of the surfactant aggregates in the complex using SHN.

3.5 Tuning the structure of CTAB-DNA complex with SHN

As discussed in section 3.3, SHN modifies the spontaneous curvature of CTAB micelles. For α (= [SHN]/[CTAB]) < 0.64, the aggregates form worm-like micelles in dilute solution. At $\alpha \approx 0.64$, the aggregates transform from cylinders to bilayers [26, 27]. We have investigated the influence of SHN on the structure of the complex by varying α. At $\alpha = 0.2$, three peaks are observed in the small angle region which can be indexed on a hexagonal lattice (fig 3.11a).

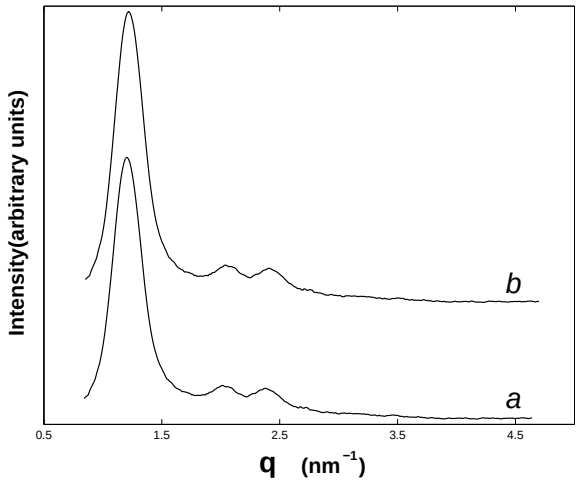

Figure 3.11: Diffraction patterns of the CTAB-SHN-DNA complexes. α = ([SHN]/[CTAB])= 0.2 and ρ (=weight of CTAB/weight of polyelectrolyte) for the different curves are:7.2 (a); 1.2 (b); ρ_{iso}=1.4 at α=0.2. CTAB concentration in the aqueous solution was 10mM.

The peak positions remain independent of DNA concentration (fig 3.11b). Up to α = 0.55, we find a similar behaviour in CTAB-SHN-DNA complexes, at different DNA concentrations (fig. 3.12). However, the lattice parameter a increases gradually with α from $a = 5.64 \pm 0.09$ nm at $\alpha = 0$ to $a = 6.06 \pm 0.09$ nm at $\alpha = 0.55$ in the hexagonal phase of the complex (fig. 3.13).

At $\alpha = 0.6$, x-ray diffraction gives two sharp peaks in the small angle region with their scattering vector q in the ratio 1: 2 (fig 3.14). In addition to this, a broad peak is observed at small angles (indicated by an arrow in the fig 3.14) whose position shifts to larger q values

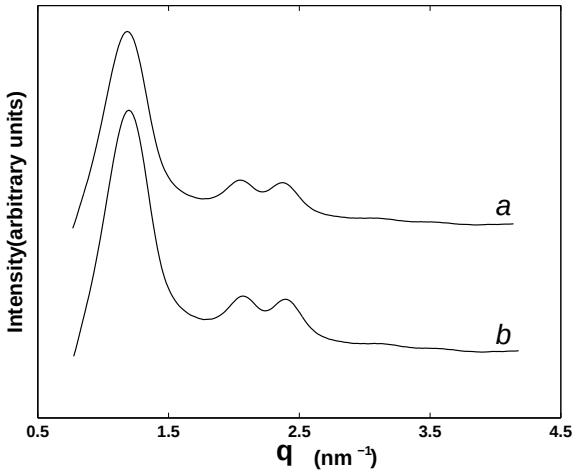

Figure 3.12: Diffraction patterns of the CTAB-SHN-DNA complexes.α= 0.55. ρ for the different curves are: 14.4 (a); 1.2 (b); ρ_{iso}=1.72 at α=0.55.

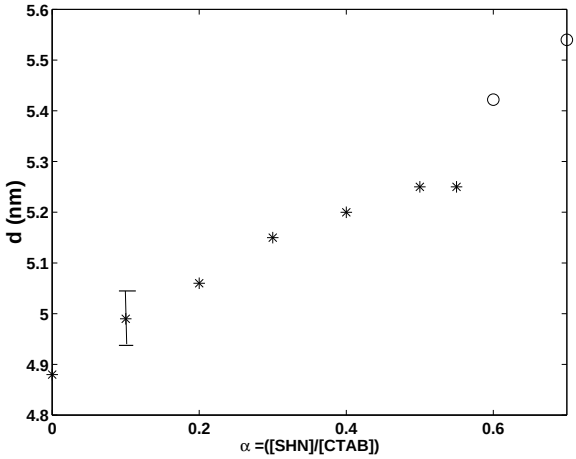

Figure 3.13: Variation of the lattice parameter with α. '*' denotes the hexagonal phase of the complex and 'o' denote the lamellar phase.

on increasing DNA concentration. The former set of peaks that remain independent of DNA content, correspond to a lamellar structure. The diffused peak is the DNA-DNA peak that has been observed earlier in lipid-DNA systems. Hence a hexagonal to lamellar transition of the complex occurs at around α = 0.6 . The lamellar periodicity at α = 0.6 is 5.45 ± 0.09 nm. A sharp decrease in d_{DNA} is observed for $\rho < \rho_{iso}$ (fig 3.15). A similar structure is also observed at α =0.7 (fig 3.16). Here the lamellar periodicity increases by 0.1 nm. The dependence of d on α is given in fig 3.13. The various phases observed in the CTAB-SHN-DNA complexes and their corresponding lattice parameters at different SHN concentrations are given in table

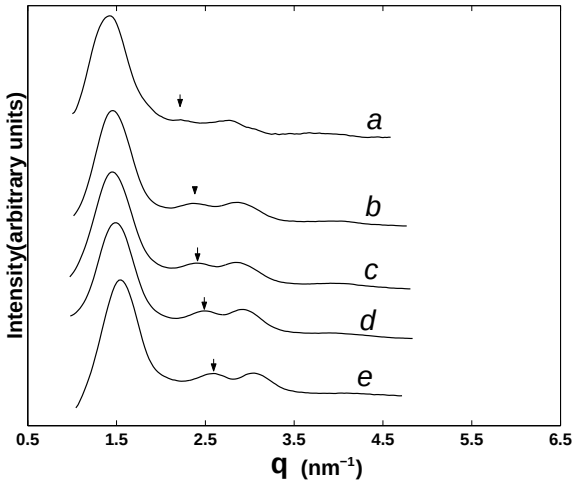

Figure 3.14: Diffraction patterns of the CTAB-SHN-DNA complexes. α= 0.6 . ρ for the different curves are: (a) 2.25; (b) 2.0; (c) 1.64; (d) 1.33; (e) 1.0; The arrow on the curves indicate in-plane DNA-DNA correlation peak. ρ_{iso}=2.8 at α=0.6.

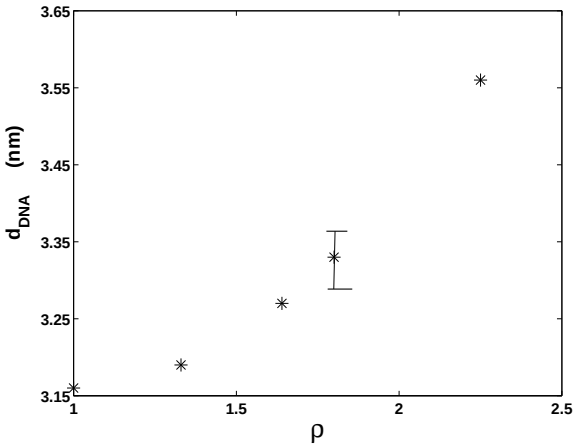

Figure 3.15: Variation of the DNA-DNA peak with ρ at α =0.6. ρ_{iso}= 2.8

3.2. No structural transformations are observed on heating up to 90 ^{o}C, although the lattice parameters are found to decrease with increasing temperature.

We have also studied the influence of NaCl on the structure of the complex. In the lamellar phase of the complex, corresponding to α = 0.6 and ρ = 1.3, the separation between the bilayers increases from 5.45 nm to 5.85 nm in the presence of 0.5 M NaCl. Also a shift in the DNA-DNA peak from 3.19 nm to 3.56 nm is observed. This is similar to the behaviour seen in lipid-DNA complexes [10].

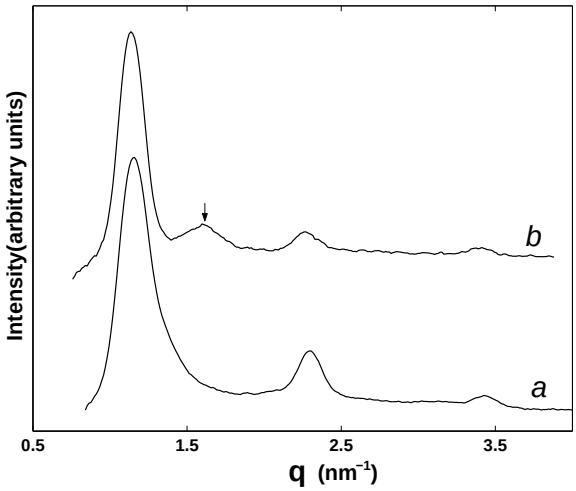

Figure 3.16: Diffraction patterns of the CTAB-SHN-DNA complexes. α = = 0.7 . ρ for the different curves are: 14.4 (a); 3 (b).The arrow on curve b indicates in-plane DNA-DNA correlation peak, ρ_{iso}=3.74 at α=0.7 .CTAB concentration in the aqueous solution was 10mM.

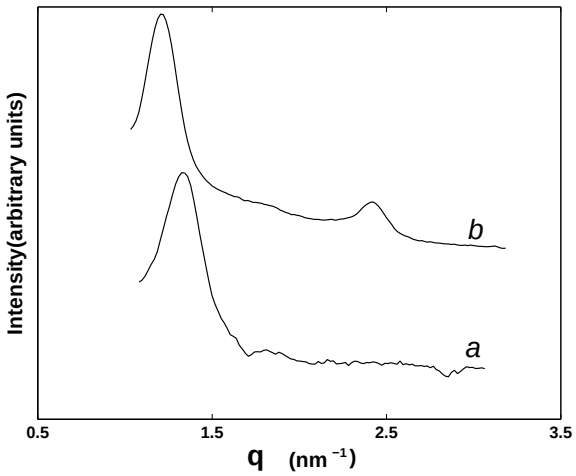

Figure 3.17: Diffraction patterns of the CTAB-ss DNA complexes. α and ρ for the different curves are: 0, 14.4 (a); 0.6, 14.4 (b); ρ_{iso}=1.12 at α=0 and ρ_{iso}=2.8 at α=0.6.

To study the influence of flexibility of the polyelectrolyte on the structure of CTAB-DNA complexes, the double stranded (ds) DNA was replaced by single stranded (ss) DNA. The persistence length of ss DNA (~ 1.5 nm) is an order of magnitude lower than that of ds DNA. CTAB-ss DNA complexes are found to form a hexagonal phase with a lattice parameter of 5.47 nm (fig 3.17a). At high SHN concentrations, (α = 0.6), the complex exhibits a lamellar phase with a periodicity of 5.15 nm (fig 3.17b).

Table 3.2: The d-spacings and structures observed in CTAB-SHN-DNA complexes at different values of α. T is the temperature.

α	$d_1(nm)$	$d_2(nm)$	$d_3(nm)$	structure	T($^\circ C$)
0	4.88	2.82	2.44	H_I^C	30
0	4.7	-	-	H_I^C	90
0.1	4.99	2.88	2.50	H_I^C	30
0.2	5.06	2.92	2.53	H_I^C	30
0.3	5.15	-	2.575	H_I^C	30
0.4	5.2	-	2.6	H_I^C	30
0.5	5.2	-	2.6	H_I^C	30
0.55	5.25	3.03	2.63	H_I^C	30
0.6	5.42	2.71	-	L_α^C	30
0.6	5.09	-	-	L_α^C	75
0.7	5.54	2.77	1.85	L_α^C	30

3.6 Discussion

The hexagonal structure observed at low SHN concentrations, should be similar to that seen in CTAB-DNA complexes. However, by adding SHN to the CTAB solution, we decrease the spontaneous curvature of the cylinders. Hence the increase in the lattice parameters of the hexagonal phase on increasing α could be the consequence of an increase in the radius of the micellar cylinders.

The lamellar periodicity of 5.45 nm at α =0.6 is consistent with the model of DNA strands sandwiched between the bilayers, with d =$\delta_m + 2R_{DNA}$, where δ_m ($\sim$ 3 nm) is the thickness of CTAB-SHN bilayer and R_{DNA} is the radius of a hydrated DNA strand (= 1.25 nm). Hence the lamellar phase obtained for the CTAB-SHN-DNA complex (fig. 3.18) is similar to the intercalated lamellar phase observed in lipid-DNA systems. In the lamellar phase of the complex, the separation between the DNA strands (d_{DNA}) depends on ρ, which is also consistent with the observations on lipid-DNA complexes [10]. The absence of DNA-DNA peaks in the lamellar complexes for $\rho > 2.25$ is probably because they fall within the first order lamellar

peak. This peak, however, appears as it shifts to higher q values for $\rho < 2.25$.

As discussed in section 3.2 in the context of DOTAP-DOPE-DNA complexes, electrostatics prefers H_{II}^C over L_α^C structure. The geometry of the H_{II}^C structure brings the surfactant ions closer to the negative charges on the DNA. Hence there is a gain in free energy due to the efficient neutralization that occurs in the H_{II}^C phase. But the free energy gain should compensate for the energy cost required to bend the surfactant monolayer around the DNA strand. If CTAB-DNA complexes formed an H_{II}^C structure, addition of SHN would reduce the energy cost required to have a negative spontaneous curvature at the micelle-water interface. Thus the presence of SHN should stabilize the inverted phase. We assume here that SHN does not substantially increase the rigidity of the bilayers. However, as discussed in section 3.4, a hexagonal to lamellar transition of the complex is observed close to where the cylinders transform to bilayers in the dilute surfactant solutions (ie at $\alpha = 0.6$). Hence these observations indicate that the structure of the complex is determined by the morphology of the aggregates in the surfactant solution. We also conclude from here that the CTAB-DNA complexes form an intercalated hexagonal phase consisting of DNA strands surrounded by cylindrical micelles (fig 3.7). The preference for this phase also indicates that the energy cost to disrupt the cylindrical micelles is much higher than the energy gain due to the greater proximity of surfactants to the DNA strand in the H_{II}^C structure. These results are consistent with the structure proposed from the analysis of diffraction data in section 3.3.

The complexes of CTAB with ss DNA also form a hexagonal phase similar to that of ds DNA. Since the persistence length of ss DNA differs from ds DNA, by an order of magnitude (refer table 1.1), the structure is expected to consist of cylindrical micelles bridged by the flexible DNA strands. In addition to the flexibility, the bare charge density of ss DNA is also different from that of ds DNA. Yet the structures obtained for the complexes are similar for the same SHN concentrations. The difference in the lattice parameters may arise due to the steric size of ds DNA that keeps the bilayers or cylinders from coming closer as compared

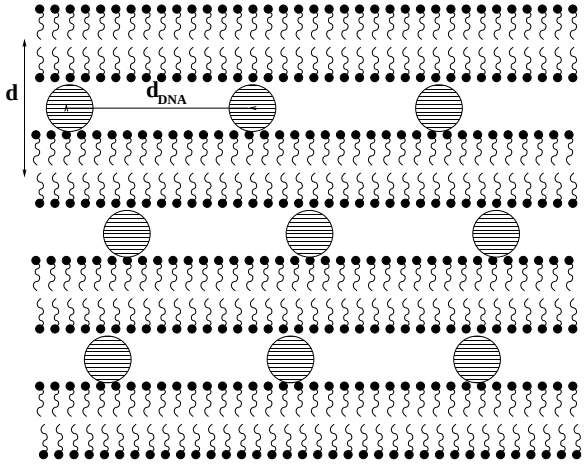

Figure 3.18: Schematic of the structure of the lamellar phase of DNA-surfactant complexes. The shaded circles represent the cross-section of the DNA strands.

to the ss DNA.

3.7 Conclusions

The complexes formed by ds and ss DNA with CTAB have a hexagonal structure. Analysis of the diffraction data indicates that the CTAB-ds DNA complex forms an intercalated hexagonal phase consisting of DNA strands surrounded by cylindrical micelles. We have further substantiated the structure by tuning the shape of the micellar aggregates using SHN. We find a continuous increase in the lattice parameter in the hexagonal phase of the complex and a hexagonal to lamellar transition at $\alpha \sim 0.6$, close to the cylinder to bilayer transition of the surfactant aggregates in dilute solutions. Both ds and ss DNA are found to exhibit a similar behaviour. We may conclude from here that the structure of the CTAB-DNA complexes is not significantly influenced by the flexibility or bare charge density of the polyelectrolyte, but is primarily determined by the morphology of the surfactant aggregates.

Bibliography

[1] P. L. Felgner and G. Rhodes, Nature **349**, 351 (1991).

[2] P. L. Felgner, Proc. Natl. Acad. Sci. U.S.A. **84**, 7413 (1987).

[3] J. Gustafsson, G. Arvidson, G.Karisson, and M. Almgren, Biochim. Biophys. Acta **1235**, 305 (1995).

[4] B. Sternberg, F. L. Sorgi, and L. Huang, FEBS Lett. **356**, 361 (1994).

[5] J. O. Raedler, I. Koltover, T. Salditt, and C. R. Safinya, Science **275**, 810 (1997).

[6] D. Lasic, H. Strey, C. A. Stuart, R. Podgornik, and P. M. Frederik, J. Am. Chem. Soc. **119**, 832 (1997).

[7] T. Salditt, I. Koltover, J. O. Raedler, and C. R. Safinya, Phys. Rev. E **58**, 889 (1998).

[8] F. Artzner, R. Zantl, G. Rapp, and J. O. Raedler, Phys. Rev. Lett. **81**, 5015 (1998).

[9] L. Golubovic, T. C. Lubensky, and C. S. O'Hern, Phys. Rev. E **62**, 1069 (2000).

[10] I. Koltover, T. Salditt, and C. R. Safinya, Biophys. J. **77**, 915 (1999).

[11] R. Bruinsma, Eur. Phys. J. B. **4**, 75 (1998).

[12] I. Koltover, T. Salditt, J. O. Raedler, and C. R. Safinya, Science, **281**, 78 (1998).

[13] J. M. Seddon, Biochim. Biophys. Acta, **1031**, 1 (1989).

[14] S. M. Gruner, J. Phys. Chem. **93**, 7562 (1989).

[15] D. Harries, S. May, W. M. Gelbart, and A. Benshaul, Biophys. J., **75**, 159 (1998).

[16] S. May, D. Harries, and A. Benshaul, Biophys. J **78**, 1681 (2000).

[17] N. Stein, G. Herren, and B. Keller, Plant Breeding **120**, 354 (2001).

[18] G. Manfioletti and C. Schneider, Nucleic Acids Research **16**, 2873 (1988).

[19] A. V. Gorelov, E. D. Kudryashov, J. Jacquier, D. M. McLoughlin, and K. A. Dawson, Physica A **249**, 216 (1998).

[20] S. Morrissey, E. D. Kudryashov, K. A. Dawson, V. A. Buckin, Progr Colloid Polym Sci. **112**, 71 (1999).

[21] S. M. Mel'nikov, V. M. Sergeyev, K. Yoshikawa, H. Takahashi, and I. Hatta, J. Chem. Phys. **107**, 6917 (1997).

[22] R. Ghirlando, E. J. Watchtel, T. Arad, and A. Minsky, Biochemistry **31**, 7110 (1992).

[23] D. Langevin, Private Communication.

[24] D. Sherwood, *Crystals, X – rays* and *Proteins*, Longman, 1976.

[25] F. Reiss-Husson and V. Luzzati, J. Phys. Chem. **68**, 3504 (1964).

[26] B. K. Mishra, S. D. Samant, P. Pradhan, S. B. Mishra, and C. Manohar Langmuir, **9**, 894 (1993).

[27] K. Horbaschek, H. Hoffmann and C. Thunig, J. Colloid Interface Sci. **206**, 439 (1998).